An Improved Calibration Approach for Travelling Wave Ion Mobility Spectrometry: Robust, High-Precision Collision Cross Sections

K. Richardson[*,†,¶], D. Langridge[†,¶], S. M. Dixit[‡,¶,τ] and B. T. Ruotolo[*,‡]

†Waters Corporation, Stamford Avenue, Altrincham Road, Wilmslow, UK

‡Department of Chemistry, University of Michigan, University Ave., Ann Arbor, MI, USA

¶These authors contributed equally to this work

E-mail: keith_richardson@waters.com; bruotolo@umich.edu

ABSTRACT: The combination of ion-mobility (IM) separation with mass spectrometry (MS) has impacted global measurement efforts in areas ranging from food analysis to drug discovery. Reasons for the broad adoption of IM-MS include its significantly increased peak capacity, duty-cycle, and ability to reconstruct fragmentation data in parallel, all of which greatly enable the analyses of complex mixtures. More fundamentally however, measurements of ion-gas molecule collision cross sections (CCS) are used to support compound identification and quantitation efforts, as well as study the structures of large biomolecules. As the first commercialized form of IM-MS, Travelling Wave Ion Mobility (TWIM) devices are operated at low pressures (~3 mbar) and voltages, are relatively short (~25cm), and separate ions on a timescale of tens of milliseconds. These qualities make TWIM ideally suited for hybridization with MS. Owing to the complicated motion of ions in TWIM devices however, IM transit times must be calibrated to enable CCS measurements. Applicability of these calibrations has hitherto been restricted to primarily singly-charged small molecules and some classes of large, multiply-charged ions under a significantly narrower range of instrument conditions. Here, we introduce and extensively characterize a dramatically improved TWIM calibration methodology. Using over 2500 experimental TWIM datasets, covering ions that span over 3.5 orders of magnitude of molecular mass, we demonstrate robust calibrations for a significantly expanded range of instrument conditions, thereby opening up new analytical application areas and enabling the expansion of high-precision CCS measurements for both existing and next-generation TWIM instrumentation.

Surveys of biomolecular interactions in living cells suggest the presence of large intertwined networks that are critical to almost all cellular processes.[1-7] Studying the roles and significance of such interactions is fundamental for understanding systems biology, disease mechanisms, and developing new therapeutics to combat human disease. A critical step in understanding the functions of biomolecular complexes is determination of their structure. This can be challenging as many biologically relevant compounds and assemblies are found in very low quantities within cells, are usually heterogenous, and may not exhibit strong binding affinities.[8,9] Our efforts to catalog and classify various networks, as well as understanding their biophysical properties, are limited mostly by the lack of technologies capable of assessing such interactions in a high-throughput and reproducible manner.[9,10] One technique that shows great promise for overcoming such limitations is mass spectrometry (MS), which has been routinely implemented to study a wide range of functional biomolecules, including metabolites, proteins, and nucleic acids.[11,12] Areas of inquiry including metabolomics[13,14], lipidomics[15], and proteomics[16,17] have recently undergone dramatic expansions fueled by MS technologies that have enabled the creation of increasingly detailed maps of biomolecular interaction networks.

A relatively recent technological addition to the pursuit of system-level biological insight is ion mobility (IM) coupled to MS (IM-MS)[18-21], which combines a gas-phase separation of analytes according to their size, shape and charge with MS detection. IM works by introducing ions into a separation chamber which contains neutral gas at a controlled pressure. Under the influence of a weak electric field (E), ions undergo collisions with gas molecules. The instantaneous velocity of an ion in the IM chamber consequently depends on the local electric field and its mobility *K*, which is in turn related to its ion-neutral collisional cross section (CCS).[22] Some IM platforms capable of providing measurements of CCS values are drift-tube IM (DTIM), travelling-wave IM (TWIM), differential mobility analyzers (DMA), and trapped IM (TIM).[23] Several research groups have used IM-MS to build libraries of CCS values[24-28] to be used as descriptors for identifying molecules or constraints for generation of three-dimensional models.[29,30] While such databases are of significant utility, difficulties can be encountered when harmonizing measurements acquired using disparate IM methods.[26] For example, while the Mason-Schamp relationship[31] describes DTIM directly, TWIM arrival times must be calibrated before CCS measurements can be obtained.[32] Although the current TWIM calibration approach is straightforward and robust for small, singly-charged molecules, more general CCS calibrations covering a wider range of ion sizes and charge states can prove challenging, as appropriate calibrants and experimental conditions must be chosen for a given experiment.[32]

TWIM, since its introduction in 2004[33] and commercialization in 2006[34], has been one of the most widely used IM platforms in academia and industry.[23] TWIM separates ions using a series of DC waves in a gas-filled RF-confining stacked-ring ion guide. Ions of higher mobility are overtaken by the waves less often than lower-mobility species and travel faster, thus enabling a mobility-based separation.[35] This concept has given rise to multiple generations of IM-MS platforms and has enabled recent advances in IM-MS technology that permit ultra-high IM resolution experiments[36,37]. Although TWIM-MS provides an excellent platform for rapid gas-phase separation of ions, the complex motion of ions in TWIM devices has prevented direct calculation of CCS values from TWIM arrival times. However, studies have shown that the average ion velocity achieved in TWIM separations correlate well with the CCS values from DTIM measurements, thus calibration methods were established.[32] There has been an increasing effort to develop a theoretical framework to understand and obtain CCS values from TWIM arrival time distributions (ATDs). In 2008, Shvartsburg *et al.*[38] derived expressions for average ion velocity and resolving power in TWIM separations. A computational framework was proposed by Mortensen *et al.*[39] in 2017 to calculate CCS values from measured TWIM arrival times. More recently, a semi-empirical relationship describing resolving power in TWIM across a range of travelling wave (TW) conditions was obtained.[40] Finally, a more complete study of the physics of TW resulted in a model for the motion of ions incorporating velocity relaxation as well as wave anharmonicity.[41] This study also proposed a calibration function incorporating velocity relaxation effects, and simulations predicted improved performance for large molecules compared with the power-law function that is currently used for TWIM CCS calibration.

In this report we describe a new TWIM calibration method that yields CCS values of dramatically improved accuracy across a wide range of analyte molecules and TW conditions. This method uses a Bayesian approach to infer CCS values using a new function incorporating the effects of velocity relaxation and the radial distribution of ions. By basing the method as closely as possible on the known physics of the instrument, we minimize the number of calibration parameters and improve the fidelity of the resulting calibration. We benchmark this novel workflow using *ca.* 20,000 calibrations created using over 2500 experimental datasets including measurements of small molecules, lipids, peptides, proteins, and protein complexes taken under a wide range of travelling-wave conditions. Taken together, our dataset spans 3.5 decades of molecular weight and evaluates 4 separate calibration functions. Overall, we demonstrate CCS values of 2-3 fold increased precision, over nearly all TWIM separation conditions, using a simple combination of five ions for external calibration. Furthermore, our new formalism enables comprehensive CCS calibrations under TW conditions previously inaccessible by any method (e.g. wave height or velocity ramping) and extends to next-generation TWIM technologies (e.g. Cyclic IMS). This new approach is supported by a software package designed to enable its rapid adoption and use by the IM-MS community.

METHOD SECTION

THEORY AND MODELLING OF TRAVELLING WAVE ION MOBILITY

In an ideal experiment, the measured transit time of an ion through a TWIM cell would be sufficient to determine its ion mobility and, consequently, its CCS. This is difficult in practice because the motion of ions in TWIM devices is complicated. Challenges include the facts that practical implementations of TWIM currently utilize waves that move forward in steps rather than smoothly, and that the temperature and pressure in the device are not usually known with sufficient accuracy. The established method of calibration of TWIM data[42] utilizes an empirically determined power-law relationship, equivalent to the following expression

$$\bar{v}_{\text{ion}} = \bar{v}_{\text{power}}(b, c) \equiv b\, K^c$$

where $\bar{v}_{\text{ion}}$ is the measured average ion velocity in the TWIM device (corrected for known time offsets), K is the ion mobility calculated using the Mason-Schamp equation, and b and c are the unknown calibration parameters[1].

The combined theoretical and modelling approach underpinning many of the advances in this study has been described elsewhere[41]. Below, we give a brief summary of the main results from this prior work together with some important new developments unique to this report. Overall, our aim is to construct a practical calibration function which reflects current understanding of TWIM ion physics. .

We begin by considering a TWIM device comprising an idealized one-dimensional, smoothly-moving travelling wave with constant wave velocity and height. In the frame of reference of the moving wave, the motion of ions can be described in dimensionless coordinates using the following differential equation of motion (see Supporting Information Section 1)

$$\alpha \underbrace{\frac{\mathrm{d}^2 z(\tau)}{\mathrm{d}\tau^2}}_{acceleration} = \underbrace{-\frac{\mathrm{d}z(\tau)}{\mathrm{d}\tau} - 1}_{motion\ against\ gas} + \underbrace{\gamma \sin z(\tau)}_{static\ wave\ potential} \qquad \#(1)$$

where $z(\tau)$ is the position of the ion as a function of the dimensionless time coordinate τ,

$$\gamma = 2\pi \frac{V_0}{v\lambda} K, \qquad \alpha = 2\pi \frac{v}{\lambda} \frac{Km}{q}, \qquad \tau = 2\pi \frac{v}{\lambda} \mathrm{t}$$

V_0 is the wave amplitude, v is the wave velocity, λ is the wavelength and m/q is the mass-to-charge ratio of the ion[2]. In small-molecule experiments under typical TWIM conditions, α is small, and the approximation $\alpha = 0$ is often appropriate. In this case, the ion velocity in the laboratory frame of reference depends only on γ and is given by

$\bar{v}_{\text{ion}} = v(1 - \omega_0)$ where $\omega_0 = \sqrt{1 - \gamma^2}$.

---

1 Physical constants and uncertainty in the pressure and temperature used in the mobility calculation can be absorbed by the parameter c, and the calibration is more usually expressed in terms of a reduced cross section and TWIM transit time.

2 This equation equivalently describes the motion of a singly-charged effective particle of mass α and unit mobility subject to a gas moving in the negative z direction with unit velocity, a linear drag force, and a static sinusoidal potential of amplitude γ.

For larger molecules however, velocity relaxation effects corresponding to ion acceleration and deceleration cannot be ignored and the measured cell transit time also depends on α and, therefore, m/q. Although (1) cannot be solved exactly in this case, it can be shown (extending previous results[41]) that for $\gamma < 1$ and small α the average ion velocity in the laboratory frame is, to order α^6,

$$\bar{v}_{\alpha,6} = v(1-\omega_0)[1-\alpha^2\omega_0^2-\alpha^4\omega_0^2(2+3\omega_0-6\omega_0^2) - \frac{1}{8}\alpha^6\omega_0^2(49+81\omega_0-205\omega_0^2-341\omega_0^3+424\omega_0^4)].$$

This expression gives velocities matching numerical solutions of (1) to within 0.5% for $\alpha < 0.4$. However, for large protein complexes we often have $\alpha \sim 1$ and $\gamma \ll 1$. We will therefore also utilise the following novel perturbative result obtained to order γ^6 using the Lindstedt-Poincaré method

$$\bar{v}_{\gamma,6} = \frac{v}{1+\alpha^2}\left[\frac{\gamma^2}{2}+\frac{\gamma^4}{8}\frac{1+10\alpha^2+15\alpha^4}{(1+\alpha^2)^2(1+4\alpha^2)} + \frac{\gamma^6}{16}\frac{1+23\alpha^2+234\alpha^4+1171\alpha^6+2291\alpha^8+1620\alpha^{10}}{4(1+\alpha^2)^4(1+4\alpha^2)^2(1+9\alpha^2)}\right],$$

which is accurate to within 0.5% for $\gamma < 0.55$. A single expression for average ion velocity (that maintains the target accuracy for all conditions that are encountered in routine TWIM experiments) is obtained by combining these expansions as follows

$$\bar{v}_{\text{blend}} = \frac{\gamma^n}{\gamma^n+\alpha^m}\bar{v}_{\alpha,6} + \frac{\alpha^m}{\gamma^n+\alpha^m}\bar{v}_{\gamma,6}, \#(2)$$

where the choice $m = 8$ and $n = 12$ maintains accuracy relative to the numerical solution, as explained in the Supporting Information Section 1. Despite their complexity, evaluation of these expressions is significantly more efficient than numerical solution of the equation of motion (1).

For the reasons given above, the motion of real ions is not exactly described by (1), and we must therefore install flexibility into (2) to allow for practical TWIM calibrations. To accomplish this, we have chosen to replace the parameters α and γ in (2) with $a\alpha$ and $g\gamma$ respectively to give a function $\bar{v}_{\text{blend}}(a,g)$. These calibration parameters are expected to have values close to 1.0 which is helpful when fitting them numerically or in assigning prior probability distributions for Bayesian inference.

In addition to the velocity relaxation effects described above, detailed modelling reveals that different populations of ions adopt different radial distributions in RF-confined TWIM devices. For example, singly-charged peptide ions are generally less well confined than multiply-charged peptide ions of the same mobility (the confining RF effective potential scales with charge while the thermal kinetic energy of the ions does not). Consequently, they are on average closer to the electrodes and effectively experience higher-amplitude travelling waves (see Supporting Information Section 2). Our analysis suggests that this effect can be approximated by multiplying the average ion velocity by a correction factor to give

$$\bar{v}_{\text{blend+radial}}(a,g,d) = e^{d/\sqrt{q}}\,\bar{v}_{\text{blend}}(a,g),$$

and

$$\bar{v}_{\text{power+radial}}(b,c,d) = e^{d/\sqrt{q}}\,\bar{v}_{\text{power}}(b,c)$$

where d is an additional calibration parameter.

Here, we investigate and compare calibrations obtained utilizing the forms $\bar{v}_{\text{power}}(b,c)$, $\bar{v}_{\text{power+radial}}(b,c,d)$, $\bar{v}_{\text{blend}}(a,g)$ and $\bar{v}_{\text{blend+radial}}(a,g,d)$. Information regarding the parameter-fitting procedures used is given in the Supporting Information Section 3.

MATERIALS AND REAGENTS

A selection of proteins (under native and denaturing conditions), peptides, lipids, small molecules and metabolites were prepared and analyzed as described in the Supporting Information Section 4.

INSTRUMENTATION

TWIM data were collected in Waters Synapt G2 IM-MS and Waters Select Series Cyclic IMS instruments. Instrumentation details can be found elsewhere[35,36]. Ions were generated using nESI, and then pulsed into the TWIM cell. For Synapt G2, voltages throughout the instrument were optimized to transmit native protein ions without significant activation. The nESI source voltage was set within the range 1.0 – 1.3 kV for all ions. Backing pressure was set at 5 mbar for native protein ions. The source temperature was set at 25 °C. The source cone and extraction cone voltages were set at 15 V and 0 V, respectively. Trap collision voltage was set at 5 V. Trap DC bias was set at a range of 35-40 V. Helium cell DC was set at 35 V. IMS bias voltage was set at 10 V. The TWIM cell (length of about 25 cm) was operated at a pressure of ~3.4 mbar (200 ml/min and 90 ml/min flow rates for He and N_2, respectively) and ATDs were collected at a range of wave height and wave velocity conditions. For cyclic IMS, data were collected using a single-pass separation with IM pressure of ~2 mbar N_2.

CCS CALIBRATION AND DATA PROCESSING

TWIM data from Synapt G2 were extracted using TWIMExtract[42]. Experimental arrival time distributions (ATDs) for most ions used in this study comprised a single Gaussian distribution indicating a single set of gas-phase conformers[38,44] (Supporting Information Section 5). Cytochrome c 7+ ions had a bimodal distribution and we used the more intense, shorter drift-time distribution. The ATDs used in this study are not affected by TWIM conditions. For peptide and protein ions, the field strengths used here remain below the low field limit[44]. Additionally, the large number of rotational and vibrational degrees of freedom in peptide and protein ions make ion heating unlikely in this study. For small molecule ions, ion heating could induce fragmentation[45]. To avoid interference from fragment ions, we extract the ATDs of the specific *m/q* values corresponding to the molecular ions.

TWIM ATDs were first convolved with a Gaussian function to simulate a resolving power of ~10 for consistency with the reference CCS data. The resulting ATDs were then fitted using a Gaussian function to determine mean arrival times. These formed the input for CCS calibrations.

Calibrations were created using the following functions: power-law; power-law+radial correction; blend; and blend+radial correction (see **Theory** section). Blend calibrations were carried out using IMSCal (available from imscal.on-demand.waters.com), a software package that uses Bayesian methods (Supporting Information Section 3) to produce calibrated CCS values and associated uncertainties. Prior probability distributions for blend function calibration parameters were assigned using a combination of theory, simulation and experimental data. Reference CCS values for calibration were taken from published databases[24,27]. Leave-one-species-out cross-validation was carried out by creating calibrant sets with one species eliminated (all charge states). The resulting calibration is then used to predict CCS values for the eliminated ions. Power-law calibrations and data analysis were carried out using NumPy and SciPy libraries[46,47].

For all-molecule calibrations, the variable a was treated as a calibration parameter. For calibrations created using smaller sets of molecules, the dimensionless parameter a was either fixed at its natural value of 1 or scaled using an empirically determined function of wave velocity v

$$a = a_0 + a_1 v$$

Where v is given in ms^{-1}, $a_0 = 0.77$ and $a_1 = 0.0004$ sm^{-1}. This linear scaling function for the variable a was empirically determined by observing the values taken by a in all-ion calibrations at various wave velocities. Fixing a reduces function overfitting with smaller datasets and for those ions where velocity relaxation is less prevalent (particularly small molecules and peptides).

Measured TWIM arrival times comprise the drift time through the mobility cell and the time for the ions to pass through subsequent gas cells, transfer optics and into the TOF analyser. We correct the measured TWIM arrival times for the time of flight into the pusher region of the TOF as described previously[42]. To account for the remaining time offset we include, in all calibration functions, an additional fitting parameter t_0. For the linear TWIM data presented here we expect $t_0 \simeq 0.6$ms. Fitted values that differ significantly from this can indicate a poor calibration. The IMSCal software package (available from: imscal.on-demand.waters.com) automates and streamlines many of the process steps outlined above, and was used throughout the later stages of our data processing efforts.

RESULTS AND DISCUSSION

Figure 1 shows a comprehensive analysis of our results, summarizing *ca.* 20,000 TWIM calibrations produced using an array of instrument conditions for a vast range of ions. The heat maps 1B-E show the percentage CCS RMSE obtained for calibrations created using all molecular species. TWIM calibrations based on blend functions, 1D and 1E, significantly outperform the original power-law approach, 1B and 1C, at almost all TWIM settings, but most strikingly at high wave velocities where velocity relaxation effects are expected to be largest. Incorporating radial corrections also results in a slight improvement of the blend results. It is remarkable that RMSE values of less than 1.7% and 1.5% are produced by the blend and blend+radial calibrations respectively.

The histograms shown in Figures 1F-I illustrate the mean and standard deviation of the CCS deviations obtained for each species when it is omitted from the calibration set and treated as an unknown over all TW conditions. The unmodified power-law approach shown in Figure 1F is unable to simultaneously produce a good calibration for proteins and small molecules when evaluated comprehensively with respect to TWIM wave height and velocity; CCS values for small molecules are underestimated while those for proteins are overestimated. When radial corrections to the power-law calibration are included (Figure 1G) the small molecule and peptide results are improved, likely because it becomes possible to better reconcile the measured CCS values of singly and multiply charged small molecules. However, CCS deviations of over 5% remain for small molecules and proteins. Both blend functions, shown in 1H and I, perform significantly better, while the blend+radial calibration (Figure 1I) gives the best overall comprehensive TWIM calibration result.

While the improvement observed for the blend+radial approach over the power-law calibration shown in Figure 1 is significant, the trends observed in the residuals (% CCS deviations) require comment. Although the residuals are small on average (below 2%), they are not stochastic. Firstly, the semi-empirical radial correction adopted here captures much, but not all, of the relevant ion transport physics. Secondly, it is not always straightforward to obtain unambiguous centroid arrival times from ATDs for large ions such as proteins, which are typically broad and prone to multimodality. Finally, we cannot rule out the presence of small (1-2%) systematic errors within the CCS databases used as reference values here (see Section 6 of the Supporting Information).

While the construction of multi-class calibrations is an important demonstration of the improved capabilities of the new approach, most TWIM applications require calibration of only a single ion class. Figure 2 contrasts the cross-validation CCS deviations obtained for all-ion calibrations with those for TWIM calibrations created within the individual ion classes. The majority of our cross-validation results are based on leave-one-species-out calibrations but, owing to the limited size of the data set, for the small molecule and denatured protein classes we use a leave-one-ion-out approach.

For the all-ion data set (Figure 2A) the two blend calibrations outperform the power-law, as in Figure 1. Since the small molecule ions studied here (Figure 2B) are singly-charged, we have omitted the results for the radially-corrected versions of the calibration functions. The power-law and blend functions perform nearly identically for this ion class, as no significant relaxation effects are predicted for ions in this m/z range. Note that almost all deviations for the calibrations performed on this ion class are less than 1%. The peptide class (Figure 2C) includes 1^+, 2^+ and 3^+ polyalanine ions, as well as 1^+ and 2^+ for the SDGRG and GRGDS peptides. As such, we predicted that TWIM CCS calibrations for this class would exhibit sensitivity to radial position effects. This is reflected in the improvement detected in both power-law and blend calibrations when radial corrections are included (absolute % CCS deviation decrease from 1.25 % to 0.46 % and 1.44 % to 0.5 % using power law and blend function, respectively, when radial correction is incorporated). Otherwise, we observe that the qualities of power-law and blend calibrations are similar. For denatured proteins (Figure 2D) power-law functions generate slightly improved TWIM CCS calibration results when compared with equivalent blend calibrations. Given the small number of denatured protein ions, and the narrow range of

CCS values exhibited by them, the small differences (~1%) between the results shown in Figure 2D should be interpreted with caution, particularly when the additional radial parameter is included. The native proteins (2E), for which we have already established the importance of velocity relaxation effects, exhibit significantly improved calibration results when the two blend functions are utilized.

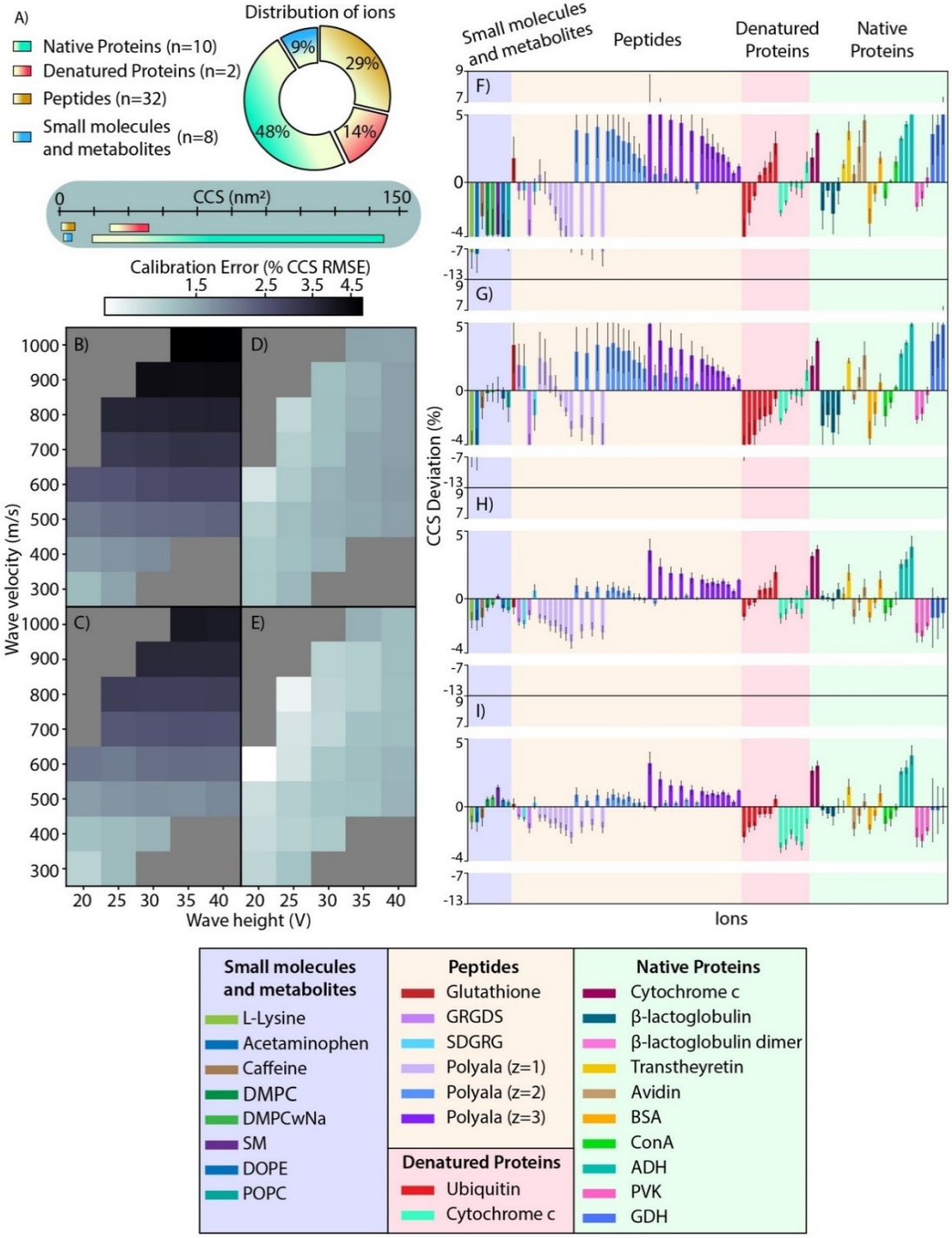

Figure 1. Performance of the calibration methods over an array of TWIM conditions. Wave height and velocity were fixed at indicated values without ramping. A) Overview of the molecular classes included. The heat maps show the dependence of % CCS RMSE calibration error on TWIM conditions using calibration expressions B) power law, C) power-law+radial correction, D) blend and E) blend+radial correction. In the blend calibrations, the parameter a was allowed to vary. Plots F-I) show the corresponding CCS deviations obtained by leave-one-species-out cross-validation. The solid bars represent averages over all TWIM conditions and the error bars show the standard deviation of the result.

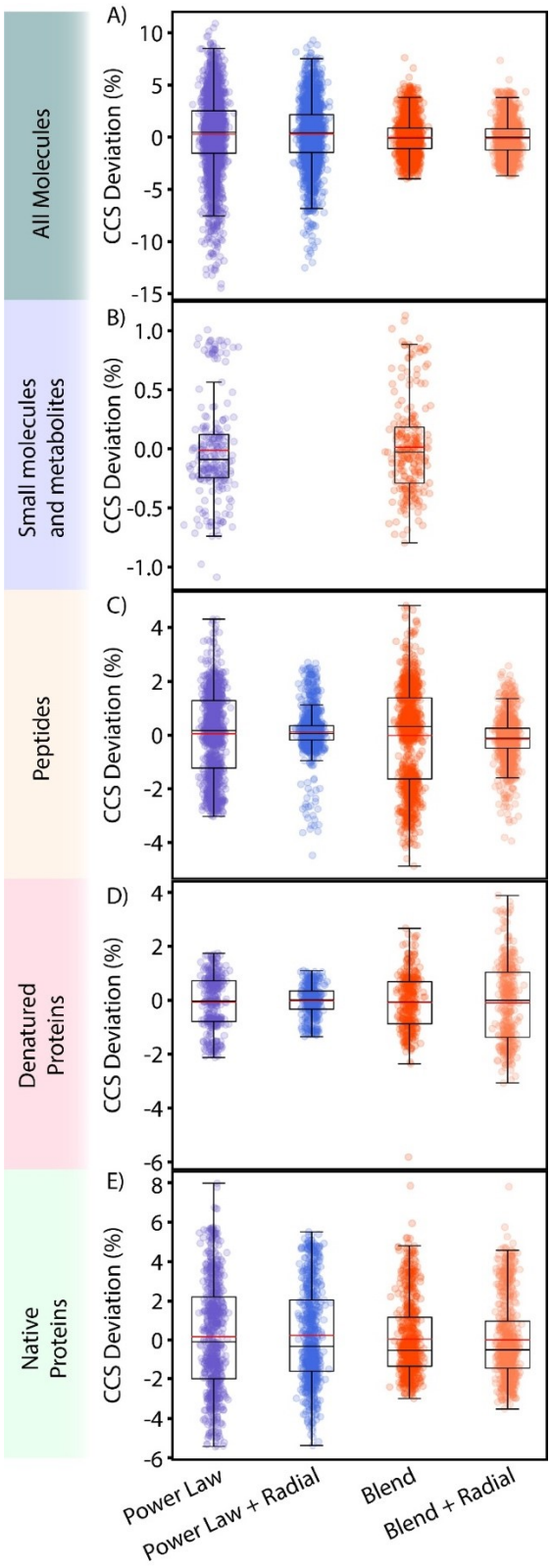

Figure 2. Comparison of all-molecule and single-molecule class calibrations produced using power-law and blend functions with and without the radial correction. Results are plotted for all TWIM settings. In the blend calibrations, the parameter a was scaled according to equation (3).

The data presented above was acquired at a series of fixed TW amplitudes and velocities. In many applications, it is useful to dynamically ramp TW conditions to optimize the spread of arrival times within the available acquisition period. Our calibration approach must be modified to accommodate such ramping and recover accurate CCS values from the resulting TWIM data. Details are provided in the Supporting Information (Section 7), and the results obtained for blend+radial calibrations under such wave height or velocity ramped conditions are comparable to those presented in Figures 1 and 2. It is important to note that high-quality power-law calibrations are not typically achieved for samples containing a wide range of multiply charged ions when wave parameters are changed dynamically during IM-MS separation. As such, the new calibration methods reported here enable the collection of high-accuracy CCS values for a significantly wider array of TWIM instrument conditions than previously possible.

Approximate helium CCS values are sometimes obtained by calibrating IM measurements obtained in nitrogen using helium reference values[42]. As might be expected, the blend-type and radially-corrected calibrations introduced here result in helium CCS values of greatly improved accuracy and precision, particularly at high TWIM wave velocities for native proteins (see Supporting Information Section 8). Furthermore, the results reported here were acquired on TWIM platforms that have near-sinusoidal traveling wave profiles, while previous generation TWIM instrument platforms (e.g. Synapt HDMS instruments) utilized pulse patterns that gave rise to highly non-sinusoidal waveforms[34]. To accommodate this, numerical rather than analytical interpolation must be used to arrive at final blended calibration terms. Results for calibrations of simulated non-sinusoidal TWIM data are given in the Supporting Information (Section 9), and significant improvements are again observed when the new calibration forms described in this report are applied to such data.

We have also applied our new calibration functions to data recorded on a cyclic TWIM instrument. By passing ions repeatedly through a curved TWIM ion guide, this instrument is capable of IM resolving powers in excess of 300.[36] Details and results for single-pass cyclic experiments are given in Section 10 of the Supporting Information. Again, use of the blend+radial function leads to a significant improvement relative to the power-law calibration. Our methods are also applicable to multi-pass data, although uncertainties in the available reference CCS values currently limit the usefulness of calibrated, high-resolution IM measurements.

Power-law TWIM CCS calibrations are typically performed using carefully selected calibrant ions that either match the molecular class of the analytes under investigation, or seek to bracket the expected ion mobilities of unknowns. The above results suggest that, for blend calibrations, it should not be necessary to carefully match calibrants to analytes. Furthermore, in routine applications, it is desirable to use a small set of calibrant species that can be prepared together in solution for rapid external calibration of IM-MS datasets acquired in a high-throughput mode. We therefore consider the viability of using a limited calibration set to create high accuracy blend+radial TWIM calibrations for use with a wide range of analytes. A mixture of large, multiply charged calibrant ions along with small molecule or peptide ions of low charge states (including 1^+ species) is needed to capture both velocity relaxation and the radial offset effects in the blend functions. Based on this requirement we selected a combination of calibrants comprising native-like BSA (14^+, 15^+, and 16^+) and reverse peptides SDGRG and GRGDS (1^+ and 2^+) ions, and used it to

create blend+radial calibrations across all TWIM conditions as discussed above. These calibrants could, for convenience, be prepared as a single solution and analyzed under native electrospray conditions.

Figure 3 shows the results obtained using this limited calibration set and the blend+radial function. The heat maps in Figure 3A-D summarise the results for small molecules and metabolites, peptides, denatured proteins and native proteins respectively. The maximum CCS RMSE observed here is 2.2%, which should be compared with a value of 1.5% obtained by calibrating using all ions present in our training set. This result demonstrates the robustness of the blend function for TWIM CCS calibrations. Power-law TWIM CCS calibrations are notoriously challenging to extrapolate to ions that possess mobilities beyond the calibration set. For the data shown in Figure 3, the largest CCS reference value used is ~4500Å^2 (BSA), while our test data contains GDH ions with CCSs of ~13500Å^2. Applying the original power-law function to this limited calibration set, we obtain a CCS RMSE of 4.6%, more than double the maximum value that we obtain with the blend+radial function. The performance of the blend+radial function is further illustrated in Figure 3E, which displays limited CCS deviation values when viewed comprehensively across all TWIM conditions. Many selections of ions that satisfy the above requirement are possible. An additional example is given in the Supporting Information Section 11.

Characterising the behaviour of these calibrations over a wide range of TWIM conditions is useful for the purposes of stress-testing TWIM calibration methods. In practice, however, TWIM conditions are typically optimized and a single set of conditions is used to perform TWIM CCS measurements. Using our comprehensive TWIM CCS calibration dataset, we surveyed all TWIM conditions to find those that lead to minimized CCS errors for each compound class using the blend+radial function while still relying on our simple calibration mixture for CCS reference ions. Figure 3F and 3G displays the results of this survey in terms of CCS relative and absolute deviation values respectively. Our data reveals that there is no single set of TWIM conditions that is optimal for CCS measurements across all analyte classes. Some trends, however, can be discerned in Figures 3A-D. For example, peptide ions favour low wave amplitudes independently of wave velocity, while the small molecules seem to favour low γ (the ratio of wave amplitude over velocity) values. The lack of any strong wave velocity dependence for native protein ions indicates that the velocity relaxation corrective aspects of the blend function are performing as expected. The statistical scatter in these results makes further assessment of any trends challenging. Nevertheless, we are able to achieve CCS deviation values of less than 1.5% across all ion classes under these optimized conditions, with the majority of data exhibiting CCS deviations between 0.5 and 1%, placing these TWIM CCS data well within the precisions recently reported for high-quality drift tube CCS values[48].

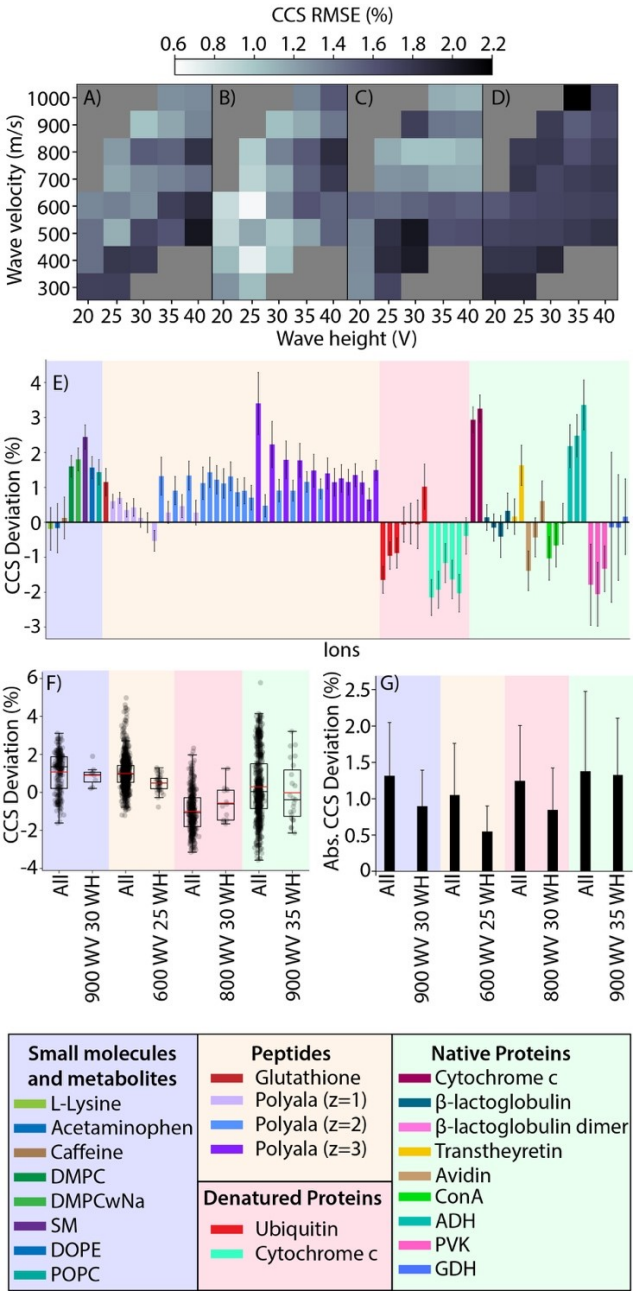

Figure 3. Blend+radial calibrations created using the minimal calibration set consisting of 14^+-16^+ charge states of native BSA and reverse peptides SDGRG and GRGDS (1^+ and 2^+). The heat maps show CCS %RMSE for each molecular class: A) small molecules and metabolites, B) peptides, C) denatured proteins, D) native proteins. E) shows CCS deviations for individual ions. F) and G) contrast results obtained for all conditions with those obtained using optimal conditions chosen for each class. The parameter a was scaled according to equation (3).

CONCLUSIONS

The results presented above support the comprehensive replacement of the power-law calibrations that have been used previously for TWIM CCS measurements with one of the new "blend" functions described here. We have demonstrated the capabilities of these new calibration functions, derived directly from analytic solutions of the TWIM differential equation of ion motion (1), across three different TWIM platforms over a range of molecular classes and TWIM settings using an extensive group of *ca.* 20,000 TWIM-MS calibrations. Further-

more, our test dataset covers ions ranging from acetaminophen (151 Da) to GDH hexamer (318,000 Da), and evaluates four different calibration functions. Our improved calibration functions have two, three or four free parameters compared with the three parameters typically used in power-law calibrations. However they generally yield more robust, accurate and precise CCS results. This is most apparent for large, multiply-charged ions under conditions for which velocity relaxation effects are significant, where wave height or velocity values are ramped, and where extrapolation of the calibration curve to CCS values that extend beyond the range of calibrant ions used is required. Optimized errors are 2-3 times lower than those currently achievable using state-of-the-art power law calibrations currently used on all TWIM-MS instruments. This means that it is possible, for the first time, to create high-quality, all-analyte TWIM calibrations using a small selection of readily-available standards.

The availability of generic calibrations at a wide range of TWIM settings is clearly enabling for high-throughput CCS measurements and removes the burden of selecting an appropriate calibrant for different ion classes or experiments. Although it is tempting to look for empirical modifications of our calibration functions that could further reduce residuals, we have resisted this impulse for two reasons. Firstly, the addition of new parameters increases the risk of overfitting, particularly given that some regions of CCS-m/z space are sparsely represented in our current calibration set. Secondly, with these improvements, the magnitude of the residuals we detect in our data is comparable to the accuracy reported for available reference CCS values (and the differences between values from different sources). It would be meaningless to report calibrated accuracies below those of the reference values (currently 1-2%). Nevertheless, the high precision of TWIM measurements (typically below 1%) combined with the increasing resolving power of modern IM instrumentation means that there is opportunity to make further progress. This will require a broader engagement by the IM community, where the careful selection and higher-accuracy measurement of appropriate reference compounds having a wide range of CCS and m/z values on multiple instrument platforms is deployed to create a new generation of IM primary standards.

ASSOCIATED CONTENT

Supporting Information Available

Further details are given in the Supporting Information PDF document. Section 1: Constructing the "Blend" Analytical Approximation. Section 2: Radial Correction to Average Ion Velocity. Section 3: Bayesian CCS Calibration. Section 4: Materials and Reagents. Section 5: Reference CCS Values. Section 6: Ramping of Travelling Wave Parameters. Section 7: Obtaining Approximate Helium CCS Values from TWIM Experimental Data Obtained in Nitrogen. Section 8: IMS Calibration on Synapt. Section 9: Calibration of Cyclic IMS data. 10: Alternative Minimal Calibration. This material is available free of charge via the Internet at http://pubs.acs.org.

AUTHOR INFORMATION

Corresponding Author

* Brandon T. Ruotolo – Email: bruotolo@umich.edu.
* Keith Richardson – Email: keith_richardson@waters.com

Present Addresses

τ Department of Pharmacology, Feinberg School of Medicine, Northwestern University, Chicago, IL USA

Author Contributions

The manuscript was written through contributions of all authors. All authors have given approval to the final version of the manuscript. ¶ These authors contributed equally.

ACKNOWLEDGMENT

TWIM theory development efforts in the Ruotolo lab are supported by the National Science Foundation Division of Chemistry under grant number 1808541 with co-funding from the Division of Molecular and Cellular Biosciences. The authors thank Jakub Ujma for his assistance in collecting the Cyclic Ion Mobility data, Kevin Giles for many helpful discussions and Leijun Song for creating the IMSCal website. The authors would like to thank Robert T. Kennedy research group at University of Michigan for providing metabolites samples and Dr. Alec Valenta for his assistance in preparing them.

REFERENCES

(1) Huttlin, E. L.; Ting, L.; Bruckner, R. J.; Gebreab, F.; Gygi, M. P.; Szpyt, J.; Tam, S.; Zarraga, G.; Colby, G.; Baltier, K.; et al. The BioPlex Network: A Systematic Exploration of the Human Interactome. Cell 2015, 162 (2), 425–440. https://doi.org/10.1016/J.CELL.2015.06.043.

(2) Feig, M.; Yu, I.; Wang, P.; Nawrocki, G.; Sugita, Y. Crowding in Cellular Environments at an Atomistic Level from Computer Simulations. J. Phys. Chem. B 2017, 121 (34), 8009–8025. https://doi.org/10.1021/acs.jpcb.7b03570.

(3) Yu, I.; Mori, T.; Ando, T.; Harada, R.; Jung, J.; Sugita, Y.; Feig, M. Biomolecular Interactions Modulate Macromolecular Structure and Dynamics in Atomistic Model of a Bacterial Cytoplasm. Elife 2016, 5. https://doi.org/10.7554/eLife.19274.

(4) Ewing, R. M.; Chu, P.; Elisma, F.; Li, H.; Taylor, P.; Climie, S.; McBroom-Cerajewski, L.; Robinson, M. D.; O'Connor, L.; Li, M.; et al. Large-scale Mapping of Human Protein–Protein Interactions by Mass Spectrometry. Mol. Syst. Biol. 2007, 3 (1), 89. https://doi.org/10.1038/msb4100134.

(5) Niphakis, M. J.; Lum, K. M.; Cognetta, A. B.; Correia, B. E.; Ichu, T.-A.; Olucha, J.; Brown, S. J.; Kundu, S.; Piscitelli, F.; Rosen, H.; et al. A Global Map of Lipid-Binding Proteins and Their Ligandability in Cells. Cell 2015, 161 (7), 1668–1680. https://doi.org/10.1016/J.CELL.2015.05.045.

(6) Piazza, I.; Kochanowski, K.; Cappelletti, V.; Fuhrer, T.; Noor, E.; Sauer, U.; Picotti, P. A Map of Protein-Metabolite Interactions Reveals Principles of Chemical Communication. Cell 2018, 172 (1–2), 358-372.e23. https://doi.org/10.1016/J.CELL.2017.12.006.

(7) Li, X.; Gianoulis, T. A.; Yip, K. Y.; Gerstein, M.; Snyder, M. Extensive In Vivo Metabolite-Protein Interactions Revealed by Large-Scale Systematic Analyses. Cell 2010, 143 (4), 639–650. https://doi.org/10.1016/J.CELL.2010.09.048.

(8) Levchenko, A. Dynamical and Integrative Cell Signaling: Challenges for the New Biology. Biotechnol. Bioeng. 2003, 84 (7), 773–782. https://doi.org/10.1002/bit.10854.

(9) Smits, A. H.; Vermeulen, M. Characterizing Protein–Protein Interactions Using Mass Spectrometry: Challenges and Opportunities. Trends Biotechnol. 2016, 34 (10), 825–834. https://doi.org/10.1016/J.TIBTECH.2016.02.014.

(10) Yang, G. X.; Li, X.; Snyder, M. Investigating Metabolite–Protein Interactions: An Overview of Available Techniques. Methods 2012, 57 (4), 459–466. https://doi.org/10.1016/J.YMETH.2012.06.013.

(11) Lössl, P.; van de Waterbeemd, M.; Heck, A. J. The Diverse and Expanding Role of Mass Spectrometry in Structural and Molecular Biology. EMBO J. 2016, 35 (24), 2634–2657. https://doi.org/10.15252/embj.201694818.

(12) Qi, Y.; Volmer, D. A. Structural Analysis of Small to Medium-Sized Molecules by Mass Spectrometry after Electron-Ion Fragmentation (ExD) Reactions. Analyst 2016, 141 (3), 794–806. https://doi.org/10.1039/C5AN02171E.

(13) Ren, J.-L.; Zhang, A.-H.; Kong, L.; Wang, X.-J. Advances in Mass Spectrometry-Based Metabolomics for Investigation of Metabolites. RSC Adv. 2018, 8 (40), 22335–22350. https://doi.org/10.1039/C8RA01574K.

(14) Zhang, X.; Quinn, K.; Cruickshank-Quinn, C.; Reisdorph, R.; Reisdorph, N. The Application of Ion Mobility Mass Spectrometry to Metabolomics. Curr. Opin. Chem. Biol. 2018, 42, 60–66. https://doi.org/10.1016/j.cbpa.2017.11.001.

(15) Hu, T.; Zhang, J.-L. Mass-Spectrometry-Based Lipidomics. J. Sep. Sci. 2018, 41 (1), 351–372. https://doi.org/10.1002/jssc.201700709.

(16) Aebersold, R.; Mann, M. Mass-Spectrometric Exploration of Proteome Structure and Function. Nature 2016, 537 (7620), 347–355. https://doi.org/10.1038/nature19949.

(17) Vidova, V.; Spacil, Z. A Review on Mass Spectrometry-Based Quantitative Proteomics: Targeted and Data Independent Acquisition. Anal. Chim. Acta 2017, 964, 7–23. https://doi.org/10.1016/J.ACA.2017.01.059.

(18) Baker, E. S.; Burnum-Johnson, K. E.; Ibrahim, Y. M.; Orton, D. J.; Monroe, M. E.; Kelly, R. T.; Moore, R. J.; Zhang, X.; Théberge, R.; Costello, C. E.; et al. Enhancing Bottom-up and Top-down Proteomic Measurements with Ion Mobility Separations. Proteomics 2015, 2766–2776. https://doi.org/10.1002/pmic.201500048.

(19) Meier, F.; Brunner, A.-D.; Koch, S.; Koch, H.; Lubeck, M.; Krause, M.; Goedecke, N.; Decker, J.; Kosinski, T.; Park, M. A.; et al. Online Parallel Accumulation-Serial Fragmentation (PASEF) with a Novel Trapped Ion Mobility Mass Spectrometer. Mol. Cell. Proteomics 2018, 17 (12), 2534–2545. https://doi.org/10.1074/mcp.TIR118.000900.

(20) Hinz, C.; Liggi, S.; Griffin, J. L. The Potential of Ion Mobility Mass Spectrometry for High-Throughput and High-Resolution Lipidomics. Curr. Opin. Chem. Biol. 2018, 42, 42–50. https://doi.org/10.1016/J.CBPA.2017.10.018.

(21) Mairinger, T.; Causon, T. J.; Hann, S. The Potential of Ion Mobility–Mass Spectrometry for Non-Targeted Metabolomics. Curr. Opin. Chem. Biol. 2018, 42, 9–15. https://doi.org/10.1016/J.CBPA.2017.10.015.

(22) Gabelica, V.; Marklund, E. Fundamentals of Ion Mobility Spectrometry. Curr. Opin. Chem. Biol. 2018, 42, 51–59. https://doi.org/10.1016/J.CBPA.2017.10.022.

(23) May, J. C.; McLean, J. A. Ion Mobility-Mass Spectrometry: Time-Dispersive Instrumentation. Anal. Chem. 2015, 87 (3), 1422–1436. https://doi.org/10.1021/ac504720m.

(24) Bush, M. F.; Hall, Z.; Giles, K.; Hoyes, J.; Robinson, C. V.; Ruotolo, B. T. Collision Cross Sections of Proteins and Their Complexes: A Calibration Framework and Database for Gas-Phase Structural Biology. Anal. Chem. 2010, 82 (22), 9557–9565. https://doi.org/10.1021/ac1022953.

(25) Struwe, W. B.; Pagel, K.; Benesch, J. L. P.; Harvey, D. J.; Campbell, M. P. GlycoMob: An Ion Mobility-Mass Spectrometry Collision Cross Section Database for Glycomics. https://doi.org/10.1007/s10719-015-9613-7.

(26) Picache, J. A.; Rose, B. S.; Balinski, A.; Leaptrot, K. L.; Sherrod, S. D.; May, J. C.; McLean, J. A. Collision Cross Section Compendium to Annotate and Predict Multi-Omic Compound Identities. Chem. Sci. 2019, 10 (4), 983–993. https://doi.org/10.1039/C8SC04396E.

(27) Bush, M. F.; Campuzano, I. D. G.; Robinson, C. V. Ion Mobility Mass Spectrometry of Peptide Ions: Effects of Drift Gas and Calibration Strategies. Anal. Chem. 2012, 84 (16), 7124–7130. https://doi.org/10.1021/ac3014498.

(28) Hines, K. M.; Ross, D. H.; Davidson, K. L.; Bush, M. F.; Xu, L. Large-Scale Structural Characterization of Drug and Drug-Like Compounds by High-Throughput Ion Mobility-Mass Spectrometry. Anal. Chem. 2017, 89 (17), 9023–9030. https://doi.org/10.1021/acs.analchem.7b01709.

(29) Paglia, G.; Angel, P.; Williams, J. P.; Richardson, K.; Olivos, H. J.; Thompson, J. W.; Menikarachchi, L.; Lai, S.; Walsh, C.; Moseley, A.; et al. Ion Mobility-Derived Collision Cross Section As an Additional Measure for Lipid Fingerprinting and Identification. Anal. Chem. 2015, 87 (2), 1137–1144. https://doi.org/10.1021/ac503715v.

(30) Eschweiler, J. D.; Farrugia, M. A.; Dixit, S. M.; Hausinger, R. P.; Ruotolo, B. T. A Structural Model of the Urease Activation Complex Derived from Ion Mobility-Mass Spectrometry and Integrative Modeling. Structure 2018, 26 (4), 599-606.e3. https://doi.org/10.1016/J.STR.2018.03.001.

(31) Mason, E. A.; Schamp, H. W. Mobility of Gaseous Ions in Weak Electric Fields. Ann. Phys. (N. Y). 1958, 4 (3), 233–270. https://doi.org/10.1016/0003-4916(58)90049-6.

(32) Gabelica, V.; Shvartsburg, A. A.; Afonso, C.; Barran, P.; Benesch, J. L. P.; Bleiholder, C.; Bowers, M. T.; Bilbao, A.; Bush, M. F.; Campbell, J. L.; et al. Recommendations for Reporting Ion Mobility Mass Spectrometry Measurements. Mass Spectrom. Rev. 2019, 38 (3), 291–320. https://doi.org/10.1002/mas.21585.

(33) Giles, K.; Pringle, S. D.; Worthington, K. R.; Little, D.; Wildgoose, J. L.; Bateman, R. H. Applications of a Travelling Wave-Based Radio-Frequency-Only Stacked Ring Ion Guide. Rapid Commun Mass Spectrom 2004, 18 (20), 2401–2414. https://doi.org/10.1002/rcm.1641.

(34) Pringle, S. D.; Giles, K.; Wildgoose, J. L.; Williams, J. P.; Slade, S. E.; Thalassinos, K.; Bateman, R. H.; Bowers, M. T.; Scrivens, J. H. An Investigation of the Mobility Separation of Some Peptide and Protein Ions Using a New Hybrid Quadrupole/Travelling Wave IMS/Oa-ToF Instrument. Int. J. Mass Spectrom. 2007, 261 (1), 1–12. https://doi.org/10.1016/j.ijms.2006.07.021.

(35) Giles, K.; Williams, J. P.; Campuzano, I. Enhancements in Travelling Wave Ion Mobility Resolution. Rapid Commun. Mass Spectrom. 2011, 25 (11), 1559–1566. https://doi.org/10.1002/rcm.5013.

(36) Giles, K.; Ujma, J.; Wildgoose, J.; Pringle, S.; Richardson, K.; Langridge, D.; Green, M. A Cyclic Ion Mobility-Mass Spectrometry System. Anal. Chem. 2019, 91 (13), 8564–8573. https://doi.org/10.1021/acs.analchem.9b01838

(37) Deng, L; Webb, I. K.; Garimella, S. V. B.; Hamid, A. M.; Zheng, X.; Norheim, R. V.; Prost, S. A.; Anderson, G. A.; Sandoval, J. A.; Baker, E. S.; et al. Serpentine Ultralong Path with Extended Routing (SUPER) High Resolution Traveling Wave Ion Mobility-MS using Structures for Lossless Ion Manipulations. Anal. Chem. 2017, 89 (8), 4628–4634. https://doi.org/10.1021/acs.analchem.7b00185.

(38) Shvartsburg, A. A.; Smith, R. D. Fundamentals of Traveling Wave Ion Mobility Spectrometry. Anal. Chem. 2008, 80 (24), 9689–9699. https://doi.org/10.1021/ac8016295.

(39) Mortensen, D. N.; Susa, A. C.; Williams, E. R. Collisional Cross-Sections with T-Wave Ion Mobility Spectrometry without Experimental Calibration. J Am Soc Mass Spectrom 2017, 28 (7), 1282–1292. https://doi.org/10.1007/s13361-017-1669-0.

(40) Dixit, S. M.; Ruotolo, B. T. A Semi-Empirical Framework for Interpreting Traveling Wave Ion Mobility Arrival Time Distributions. J. Am. Soc. Mass Spectrom. 2019, 30 (6), 956–966. https://doi.org/10.1007/s13361-019-02133-6.

(41) Richardson, K.; Langridge, D.; Giles, K. Fundamentals of Travelling Wave Ion Mobility Revisited: I. Smoothly Moving Waves. Int. J. Mass Spectrom. 2018, 428, 71–80. https://doi.org/10.1016/J.IJMS.2018.03.007.

(42) Ruotolo, B. T.; Benesch, J.L.P.; Sandercock, A.M.; Hyung, S.-J.; Robinson, C.V. Ion mobility-mass spectrometry analysis of large protein complexes. Nat. Protocols 2008, 3 (7), 1139-1152

(43) Haynes, S. E.; Polasky, D. A.; Dixit, S. M.; Majmudar, J. D.; Neeson, K.; Ruotolo, B. T.; Martin, B. R. Variable-Velocity Traveling-Wave Ion Mobility Separation Enhancing Peak Capacity for Data-Independent Acquisition Proteomics. Anal. Chem. 2017, 89 (11), 5669–5672. https://doi.org/10.1021/acs.analchem.7b00112.

(44) Dixit, S. M.; Richardson, K.; Langridge, D.; Giles, K.; Ruotolo, B. T.; A Novel Ion Pseudo-trapping Phenomenon within Traveling

Wave In Guides. J. Am. Soc. Mass Spectrom., 2020, 31, 880-887. https://doi.org/10.1021/jasms.9b00095.

(45) Morsa, D.; Gabelica, V.; De Pauw, E. Effective Temperature of Ions in Traveling Wave Ion Mobility. Anal. Chem. 2011, 83 (14), 5775–5782. https://doi.org/10.1021/ac201509p.

(46) Walt, S. van der; Colbert, S. C.; Varoquaux, G. The NumPy Array: A Structure for Efficient Numerical Computation. Comput. Sci. Eng. 2011, 13 (2), 22–30. https://doi.org/10.1109/mcse.2011.37.

(47) Oliphant, T. E. Python for Scientific Computing. Comput. Sci. Eng. 2007, 9 (3), 10–20. https://doi.org/10.1109/MCSE.2007.58.

(48) Stow, S. M.; Causon, T. J.; Zheng, X.; Kurulugama, R. T.; Mairinger, T.; May, J. C.; Rennie, E. E.; Baker, E. S.; Smith, R. D.; McLean, J. A.; et al. An Interlaboratory Evaluation of Drift Tube Ion Mobility–Mass Spectrometry Collision Cross Section Measurements . Anal. Chem. 2017, 89 (17), 9048–9055. https://doi.org/10.1021/acs.analchem.7b01729.